AIP | Review of Scientific Instruments

Thoron detection with an active Radon exposure meter—First results

J. Irlinger, M. Wielunski, and W. Rühm

Citation: Review of Scientific Instruments **85**, 022106 (2014); doi: 10.1063/1.4865162
View online: http://dx.doi.org/10.1063/1.4865162
View Table of Contents: http://scitation.aip.org/content/aip/journal/rsi/85/2?ver=pdfcov
Published by the AIP Publishing

Thoron detection with an active Radon exposure meter—First results

J. Irlinger,[a] M. Wielunski, and W. Rühm
ISS, Helmholtz Center Munich, Research Center for Environment and Health, 85764 Neuherberg, Germany

(Received 15 September 2013; accepted 3 November 2013; published online 21 February 2014)

For state-of-the-art discrimination of Radon and Thoron several measurement techniques can be used, such as active sampling, electrostatic collection, delayed coincidence method, and alpha-particle-spectroscopy. However, most of the devices available are bulky and show high power consumption, rendering them unfeasible for personal exposition monitoring. Based on a Radon exposure meter previously realized at the Helmholtz Center Munich (HMGU), a new electronic prototype for Radon/Thoron monitoring is currently being developed, which features small size and weight. Operating with pin-diode detectors, the low-power passive-sampling device can be used for continuous concentration measurements, employing alpha-particle-spectroscopy and coincidence event registration to distinguish decays originating either from Radon or Thoron isotopes and their decay products. In open geometry, preliminary calibration measurements suggest that one count per hour is produced by a 11 Bq m^{-3} Radon atmosphere or by a 15 Bq m^{-3} Thoron atmosphere. Future efforts will concentrate on measurements in mixed Radon/Thoron atmospheres. © *2014 AIP Publishing LLC*. [http://dx.doi.org/10.1063/1.4865162]

I. INTRODUCTION

The decay products of the naturally occurring isotope ^{222}Rn, referred to as "Radon" below, have been identified to increase the excess relative risk for lung cancer[1,2] and are, after smoking, the main cause responsible for that disease.[3] This was, amongst others, deduced from epidemiological studies, in which the Radon concentration at homes[1,4] and in Uranium mines[2,5] had been correlated to increased lung cancer rates. For example, indoor studies were based on Radon concentrations in the air of sleeping and living rooms while a person's mobility was not taken into account, thus adding to the uncertainty in the deduced excess risk estimates. In order to quantify the Radon exposure of an individual, a portable electronic Radon exposure meter has been developed at the Helmholtz Center Munich (HMGU).[6] This device allows for a realistic evaluation of a person's Radon exposure when constantly worn. But despite these efforts to determine the health risk due to Radon exposure, the effects of the decay products of another Radon isotope, ^{220}Rn, commonly called "Thoron," have not been taken into account but cannot be neglected.[7,8] In fact, under certain conditions the annual dose due to Thoron can exceed that of Radon.[9,10] In contrast to Radon, the gas concentration of the short lived Thoron isotope ($t_{1/2} = 55.6$ s) is difficult to measure and advanced methods have to be applied.[11] Recent developments already combine Radon and Thoron gas measurements,[12] but most are not designed as personal exposure monitor. Based on the previously developed Radon exposimeter prototype, which features small size, low weight, and minimal power consumption, the successive steps for its optimization to a Radon/Thoron online monitor are described here. Primarily its sensitivity for Radon was enhanced, following the implementation of an alpha-particle-spectrometer with the additional method of delayed coincidence measurements. The new device was calibrated in high Radon and Thoron concentrations within a closed chamber, respectively.

II. MATERIALS AND METHODS

A. Principle

For an improved Radon gas concentration measurement the same method, as described for the previous prototype,[6] was applied. The device is based on a passive diffusion chamber with filtering medium, employing pin-diodes for alpha-particle detection. It therefore allows for continuous concentration measurements as described in the recently released ISO 11665-5:2012 standard.[13] The electronic design principle also remained unchanged. A voltage drop due to ionization currents is amplified, shaped, counted, and then stored in a microprocessor. For pure Radon detection a simple energy threshold detection via a comparator is sufficient, while for measurements in mixed Radon/Thoron environments more information on the alpha particle energy is necessary. Here two new developments are described in order to enhance the Radon sensitivity and enable simultaneous Radon/Thoron detection. First, the active detection area was increased by means of larger detectors, requiring a redesign of the amplification stage. Second, to allow for alpha-particle spectrometry, an analog-to-digital converter (ADC) of a newly embedded microprocessor was used. In the following only the newly designed parts of the device will be discussed.

B. Technical realization

1. Detector

A new detector for the special requirements of alpha-particle detection has been developed at the Institute of Electron Technology in Warsaw.[14] The detector features an active detection area of approximately 467 mm^2, covered with a 400 nm thick aluminum layer acting as cathode, and a

[a]josef.irlinger@helmholtz-muenchen.de

depleted active layer thickness of 110 μm. This ensures that charges from ionizing alpha-particles with energies of less than or equal to 10 MeV, which have a maximum penetration depth of 70 μm according to SRIM[15] calculations, are fully collected.

The employed detectors have been tested for their energy absorption behavior, which in a first order approximation can be assumed to be linear. For this the monitoring system has been put into a low pressure environment at 13 mbar and 6 detectors were individually exposed with alpha-particles from an Americium-Curium-Plutonium source, with fixed detector-source distance (19.2 mm). The obtained spectra were apart statistical fluctuations similar and therefore summed up for evaluation. The expected peaks at 5.24 MeV, 5.49 MeV, and 5.90 MeV were clearly visible and each was fitted by a Gaussian function, resulting in a mean channel number per incident energy. The linear regression of the obtained values yielded a coefficient of determination of $R^2 = 0.974391$, confirming the assumption of an almost linear energy absorption.

In the monitoring system two of the detectors are connected in parallel with a reverse bias voltage of 14 V and a capacitance of 470 pF each. As an approximation the voltage drop at the detectors, due to currents generated by electron-hole pair production of the absorbed alpha-particles, can be calculated via Eq. (1):

$$\Delta U = \frac{E_\alpha e}{E_{ehp} C}, \tag{1}$$

where ΔU is the induced voltage drop, E_α is the alpha particle energy, e is the elementary charge, E_{ehp} is the electron-hole-pair production energy, and C is the combined capacitance of the detectors. With an energy of 3.63 eV per electron-hole pair[16] the voltage drop for the targeted α-particle energy range between 1 and10 MeV approximately spans from 47 to470 μV, and is therefore too small to be measured directly. Hence a new amplifier had to be developed with high gain and linear amplification which is discussed next.

2. Amplifier

The amplification system uses three stages for amplifying and shaping the signal produced by an α-particle. The system is entirely built from discrete components to allow for a maximum optimizability concerning power consumption and gain. The pre- and main amplifier employ n-channel field effect transistors (FETs), which are characterized by a high input impedance along with low output noise. Therefore, FETs are ideally suited for small input signals such as those described above. The preamplifier uses a negative feedback to stabilize its gain with rise and decay time constants of 0.14 μs and 100 μs, respectively. In order to prevent pile-up from successive signals, a RLC shaping unit follows, transforming the signal to semi-Gaussian shape with a full-width-half-maximum (FWHM) pulse width of 14 μs. As this signal is only in the output range from 5 to 50 mV, the last closed-loop amplification stage boosts the signal to its final output voltage range of $64 - 644$ mV for energies $1 - 10$ MeV, respectively. The linearity of the whole system has been checked via pulser method, which electronically induces voltage drops at the detectors as calculated in Eq. (1). A linear regression of the obtained output voltage amplitudes with respect to input energy in MeV yields a slope of 63.0 mV MeV^{-1} with a coefficient of determination of $R^2 = 0.999971$. The total current consumption of the amplifier system is approximately 375 μA in idle state.

3. Microcontroller

As new microprocessor (MCU) a MSP430 F2419 was utilized. It has several advantages compared to the previously used MCU as it offers a 16-bit reduced instruction set computing (RISC) architecture with 16 MHz clock frequency, 12-bit ADC, 4 kB of RAM, and 120 kB of memory. It features low power modes that require only a minimum of current in the range of 10 μA for data retention. However, due to the non-deterministic source of the signal, the ADC has to be switched on all the time requiring a relative huge steady input power, typically of the order of 2 mW. Further, it features several high precision timers which can be used for delayed coincidence measurements. As trigger the internal comparator is used in a Schmitt-Trigger setup with a threshold voltage of 82 mV. On activation, the pulse is sampled 4 times by the ADC with a sampling interval of 3.6 μs. The acquired number is proportional to the pulse area, and therefore to the incident α-particle energy. The ADC uses its internal 1.5 V reference voltage, resulting in a voltage resolution of 0.4 mV per channel which corresponds to an energy of 6 keV per channel. But as the whole system is subjected to noise, the measured energy resolution, which is the FWHM of the acquired Gaussian peaks during pulser calibration, corresponds to $\Delta E \approx 130$ keV. Data transfer is bi-directional, using universal asynchronous receiver/transmitter (UART) protocol with a universal serial bus (USB) converter at speeds of 115 kbaud. Measurement interval and start can be set via a PC, acquired data are not lost in case of power failure. The total current consumption of the chip and its dependencies is approximately 545 μA.

4. Casing

The two detectors and all electronic components are placed on the same printed circuit board (PCB) within an aluminum casing (Hammond Electronics 27134PSLA, length: 11.1 cm, width: 6.0 cm, height: 3.2 cm) to shield the electronics and ensure electromagnetic compatibility (EMC). For Radon gas measurements the board is fixed on the cover of the casing. In the cover 6 holes with 4 mm diameter were drilled, and in between the cover plate and the fixed PCB an electro-conductive sponge was compressed for filtration. For the measurements in a mixed Radon/Thoron atmosphere, the dimensions were the same, but instead of diffusion holes in the cover plate, the top plate of the casing itself was perforated. In this setup the detectors directly faced the inlets, to minimize the diffusion path between inlet and detection area. For these very first measurements no filter was used.

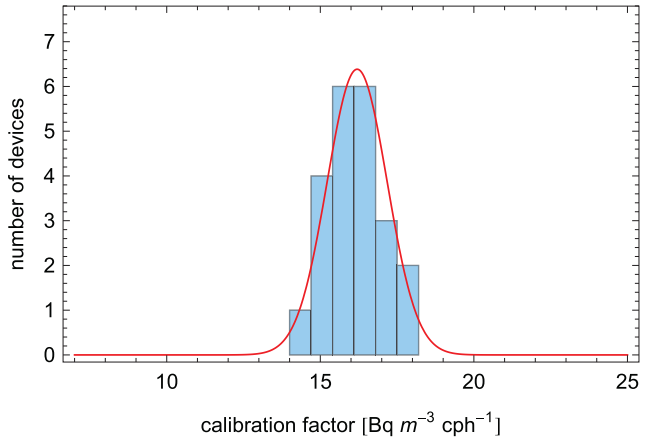

FIG. 1. Distribution of calibration factors with bin width of 0.7 and Gaussian fit (solid line).

III. RESULTS AND DISCUSSION

A. Radon calibration

With the improved amplifier and detector layout 22 new Radon monitor prototypes have been built. The devices have been calibrated in a high Radon concentration environment (up to 2300 Bq m^{-3}) within a closed vessel, using Uranite as Radon source. As reference device an AlphaGuard® was used. The comparator energy threshold for the devices was set to 1.8 MeV. Generally, the uncertainty associated with the calibration factor of a single device is governed by the number of counts detected. In the present experiment this uncertainty was about 9.0%. Figure 1 shows the distribution of the obtained calibration factors. With a mean value of 16.2 ± 0.9 Bq m^{-3} cph^{-1} (mean ± standard deviation), the sensitivity of the device, compared to the previous one, was almost doubled. Figure 1 also demonstrates that the device can be built in a reproducible manner within a small error boundary. Hence, for a series of devices it may be sufficient to calibrate only one instead of each individual device, and to assume that the resulting calibration factor is representative for the other devices, although an individual calibration is preferred.

B. Radon/Thoron spectra

Two different spectra in either a pure Radon or a pure Thoron environment have been acquired, using the newly developed digital part and the geometry with the detectors directly facing the inlets. For this Thorium containing lantern mantels were used as Thoron source, within an airtight steel pot of 54 liters volume. As the Thoron evaporation is humidity dependent, the relative humidity (RH) in the calibration pot was stabilized with a saturated potassium-carbonate solution. The prototype was put into a calibration box of 13 liters air volume, which was connected via in/outlet-pipes to the source pot. A membrane air pump with an approximate air flow of 1 l min^{-1} was switched on when the calibration was started. During the calibration the temperature and RH were monitored. For both calibration spectra the mean environmental conditions were 24.0 °C, 43.0% RH with an external pressure of 1012 − 1015 mbar. The spectra were normalized by dividing each individual acquired spectrum by the respective reference gas concentration, for which a Rad7® was used, and calculating the mean of several measurement intervals. The measurement period was 1 h each, for Radon calibration the total acquisition time was 64 to 95 h with a mean Radon concentration of 3340 ± 36 Bq m^{-3}, while for Thoron 60 to 80 h were used with a mean Thoron concentration of 8420 ± 100 Bq m^{-3}. Hence both isotopes and their

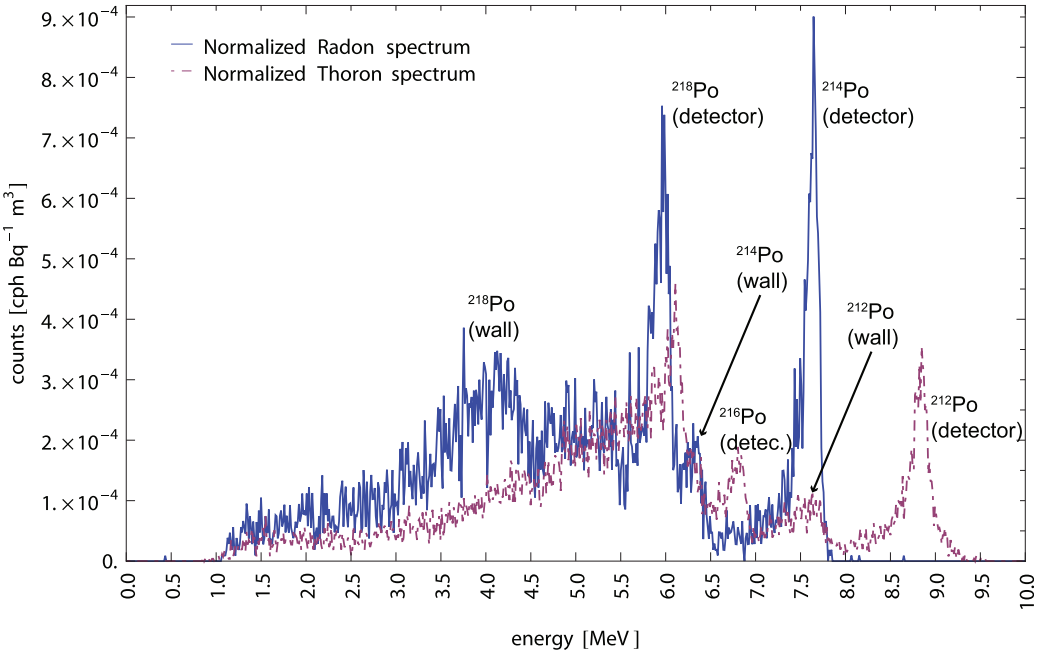

FIG. 2. Radon and Thoron spectrum of same device without filtration, in respective pure gas environments. Different decay energies due to different progenies are easily separable. "Detector" refers to progenies attached to the detector, while "wall" refers to progenies attached to casing walls. For details on nuclides please see Table II.

TABLE I. Calibration factors.

Gas	Calibration factor (Bq m^{-3} cph)	Total counts (Bq^{-1} m^3 h^{-1})	Conversion factor[a] (cm^{-2} kBq^{-1} m^3 h^{-1})
Radon	11.1	0.091	9.69
Thoron	14.9	0.067	7.18

[a]Active detection area of 9.34 cm^2.

progeny were in equilibrium. For example, ^{212} Po reaches 98% of its equilibrium activity after 60 h, therefore the spectra also represent the equilibrium conditions. In Figure 2 one can easily identify the decay peaks of the progeny attached to the detector, here called detector decays. Also alpha particle counts from daughter products attached to the casing walls are observed, designated as wall counts. The total number of counts per hour for Radon and Thoron, starting from energies at 1 MeV, is shown in Table I.

The Radon sensitivity in Table I is slightly better compared to the one shown in Sec. III A, as this device has no filter medium and a lower energy detection threshold. Comparing the results to CR-39 based passive integrating monitors,[17,18] the device presented here has an improved sensitivity by more than a factor of 3. Further, it is notable that the sensitivity of the device is almost the same for Radon and Thoron gases. However, this is expected to change drastically for Thoron when shielding the holes in the detector casing by a filter, to prevent Thoron progeny in the air to enter the detection volume. This will be evaluated in follow up measurements.

For the energy calibration of the system, the three peaks of the progenies attached to the detector surface (Fig. 2), namely, ^{218} Po, ^{214} Po, and ^{212} Po were considered, with reference energies as in Table II. The linear regression of the three values yields a slope of 11.96 keVchannel^{-1} and an offset of −264.2 keV.

Additionally, for considerations on a new geometry in future developments it is desirable to remove interference of wall decay peaks with detector attached ones, in order to get fast responses for varying gas concentrations, especially for the delayed ^{212} Po, which in this setup adds to the ^{214} Po peak (Fig. 2), and further to allow for a discrimination of decays originating either from Radon or Thoron. Furthermore, the energy loss of alpha-particles originating from decay products attached to casing walls depends on various environmental parameters such as humidity, temperature, and air pressure. Therefore, for best results wall decay counts should be avoided completely, either by a large distance between casing walls and detector (to make sure the α-particles emitted by Radon or Thoron progenies attached to the casing walls are absorbed by air before reaching the detector), or by just considering decays from progenies attached to the detector surface. The resulting lower sensitivity can be enhanced by coincidence event registration as discussed next.

C. Coincidences

Apart from the alpha-particle decay energy it is possible to acquire additional information about the Radon and Thoron decay. The method of delayed coincidence counts uses decay time differences in the Thoron and Radon decay chains (Table II). An event occurring within a certain time window Δt after the registration of a primary one is called a coincidence count. The shortest interval between two successive alpha-particle decays applies for ^{220} Rn and its daughter ^{216} Po, which has a half-life of 150 ms. There is of course a probability that random decays not connected to the successive decay of ^{220} Rn $\rightarrow$ ^{216} Po are detected within Δt, which are called chance coincidence counts. The number of chance coincidence counts n_c is connected to the total count rate n_t via Eq. (2):[20]

$$n_c = n_t \cdot (n_t - n_c) \cdot \Delta t, \tag{2}$$

$$n_c = \frac{n_t^2 \cdot \Delta t}{1 + n_t \cdot \Delta t}. \tag{3}$$

The parabola of Eq. (3) as well as the measured chance coincidence count rate in a pure Radon environment, where no natural coincidence due to Thoron can occur, are shown in Figure 3. Hence the number of real coincidences per measurement interval can be calculated by subtracting the expected chance coincidence rate (Eq. (3)) from the measured coincidence rate. As a result one gets a higher count rate which can be correlated to true Thoron decays, as which would have been possible with normal spectroscopy only. In the current setup, when setting a region of interest (ROI) at energies 6.5 − 7.0 MeV, where fast ^{216} Po decays occur with low

TABLE II. Radon/Thoron decay series.

Nuclide	Half-life[19]	E_α[19] (MeV)	Meas. E_α[a] (MeV)
^{222} Rn	3.82 d	5.49	…
^{218} Po	3.04 min	6.00	6.00
^{214} Pb	26.9 min	…	…
^{214} Bi	19.7 min	…	…
^{214} Po	164 μs	7.69	7.69
^{220} Rn	55.6 s	6.29	…
^{216} Po	150 ms	6.78	6.83
^{212} Pb	10.6 h	…	…
^{212} Bi	60.6 min	6.05	…
^{212} Po	298 ns	8.78	8.81

[a]Energy of primary progeny peaks as in Fig. 2.

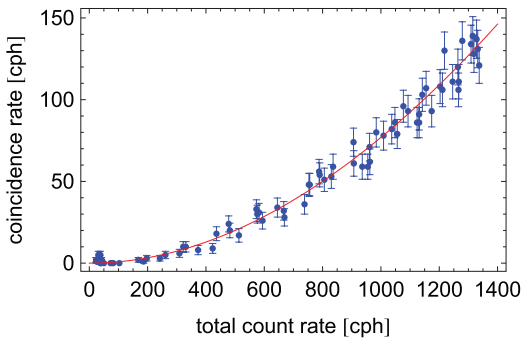

FIG. 3. Measured (dot symbols) and theoretical chance coincidence rate (solid line) in pure Radon environment calculated with Eq. (2), with $\Delta t = 320$ ms.

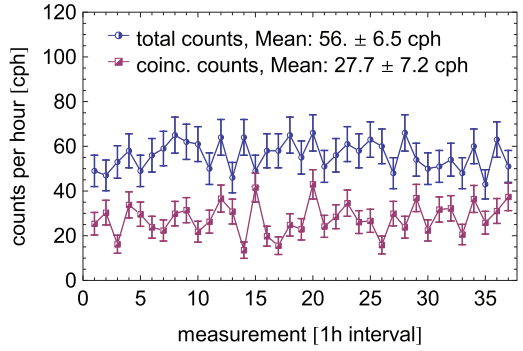

FIG. 4. Total and coincidence count rates in pure Thoron environment, for energy ROI 6.5 − 7.0 MeV of ^{212} Po.

Radon background (Fig. 2), the count rate is increased by almost 50% by coincidence counts, as shown in Figure 4. The number of total counts is the sum of coincidence and normal counts in the ROI, while the coincidence counts are integrated over an energy range of 1.0 − 7.0 MeV, subtracting the theoretical chance coincidences. In the measurement period the mean Thoron concentration was 9.6 kBq m^{-3}, resulting in a calibration factor of 114.9 Bq m^{-3} cph^{-1}, or a conversion factor of 0.93 counts cm^{-2} kBq^{-1} m^3 h^{-1}. This low sensitivity can be enhanced in future by using a different evaluation method instead of the limited energy ROI used for this example.

IV. CONCLUSION

A new electronic monitor for combined ^{222} Rn and ^{220} Rn gas concentration measurements is being developed. The low weight and small casing allows the exposure meter to be worn on person easily, while the low power consumption allows measurements periods for more than 50 days without recharge interruptions. The sensitivity of the device has been increased with respect to a previous prototype by a factor of 2. Its calibration factor for Radon is better than that of comparable electronic devices on the market, such as Sarad DOSEman[21] (52.1 Bq m^{-3} cph^{-1}) or Canary Digital Radon Monitor[22] (76.9 Bq m^{-3} cph^{-1}), and in addition is also much smaller when compared to passive CR-39 detectors. Furthermore, it allows parallel Thoron monitoring, employing alpha-particle spectroscopy and coincidence event registration, which will be further improved in the near future with respect to sensitivity and the evaluation algorithm. The influence of environmental parameters such as pressure, temperature, humidity, and aerosol particle size on detection sensitivity will also be investigated.

ACKNOWLEDGMENTS

This study was supported by the German Federal Ministry of Education and Research (Contract No. 02NUK015B). Its contents are solely the responsibility of the authors.

[1]S. Darby, D. Hill, A. Auvinen, J. M. Barros-Dios, H. Baysson, F. Bochicchio, H. Deo, R. Falk, F. Forastiere, M. Hakama, I. Heid, L. Kreienbrock, M. Kreuzer, F. Lagarde, I. Mäkeläinen, C. Muirhead, W. Oberaigner, G. Pershagen, A. Ruano-Ravina, E. Ruosteenoja, E. Schaffrath Rosario, M. Tirmarche, L. Tomáscaron, E. Whitley, H. Wichmann, and R. Doll, Br. Med. J. **330**, 223 (2005).
[2]M. Tirmarche, J. Harrison, D. Laurier, F. Paquet, E. Blanchardon, and J. Marsh, Ann. ICRP **40**, 1 (2010).
[3]H. Zeeb and F. Shannoun, *Handbook on Indoor Radon: A Public Health Perspective* (WHO, 2009).
[4]H. E. Wichmann, A. S. Rosario, I. M. Heid, M. Kreuzer, J. Heinrich, and L. Kreienbrock, Health Phys. **88**, 71–79 (2005).
[5]L. Walsh, A. Tschense, M. Schnelzer, F. Dufey, B. Grosche, and M. Kreuzer, Radiat. Res. **173**, 79–90 (2010).
[6]F. L. Karinda, B. Haider, and W. Rühm, Radiat. Meas. **43**, 1170–1174 (2008).
[7]F. Steinhäusler, W. Hofmann, and H. Lettner, Radiat. Prot. Dosim. **56**, 127–131 (1994).
[8]S. Tokonami, Radiat. Prot. Dosim. **141**, 335–339 (2010).
[9]J. Tschiersch, W. B. Li, and O. Meisenberg, Radiat. Prot. Dosim. **127**, 73–78 (2007).
[10]O. Meisenberg and J. Tschiersch, Indoor Air **21**, 240–252 (2011).
[11]C. Nuccetelli and F. Bochicchio, Radiat. Prot. Dosim. **78**, 59–64 (1998).
[12]S. Tokonami, M. Yang, H. Yonehara, and Y. Yamada, Rev. Sci. Instrum. **73**, 69 (2002).
[13]ISO, *Standards to Help Manage Risk of Exposure to Radon* (International Organization for Standardization, 2012), Vol. 11665, No. 5.
[14]M. Wegrzecki, J. Bar, T. Budzyński, M. Cież, P. Grabiec, R. Kozłowski, J. Kulawik, A. Panas, J. Sarnecki, W. Słysz, D. Szmigiel, I. Wegrzecka, M. Wielunski, K. Witek, A. Yakushev, and M. Zaborowski, Proc. SPIE **8902**, 890212-1–890212-11 (2013).
[15]J. F. Ziegler, M. D. Ziegler, and J. P. Biersack, Nucl. Instrum. Methods Phys. Res., Sect. B **268**, 1818–1823 (2010).
[16]G. F. Knoll, *Radiation Detection and Measurement* (Wiley, 2010).
[17]S. Tokonami, H. Takahashi, Y. Kobayashi, W. Zhuo, and E. Hulber, Rev. Sci. Instrum. **76**, 113505 (2005).
[18]W. Zhuo, S. Tokonami, H. Yonehara, and Y. Yamada, Rev. Sci. Instrum. **73**, 2877 (2002).
[19]C. M. Baglin and V. S. Shirley, *Table of Isotopes* (Wiley-Interscience, 1998), Vol. 1.
[20]J. Bogen, M. Sappok, and G. Schumann, Arch. Meteorol., Geophys. Bioklimatol., Ser. A **21**, 171–182 (1972).
[21]Sarad-GmbH, *DOSEman Datasheet*, http://www.sarad.de (2007).
[22]Corentium-AS, *Canary Datasheet*, http://www.corentium.com (2013).